Research Journal of Chemical Sciences ISSN 2231-606X
Vol. **16(1),** 39-51, February **(2026)** *Res. J. Chem. Sci.*

Integrated theoretical study of the inhibitory activity of (E)-3-(2-benzylidenehydrazinyl)-5,6-diphenyl-1,2,4-triazine derivatives on α-Glucosidase

Assongba Gaston KPOTIN*, Maounou Boris AMOUSSOU, Sèlonou Gautier KANKINOU, Guy Sylvain Yacole ATOHOUN
Laboratory of Physical Chemistry-Materials and Molecular Modelling (LPC3M), Unit of Theoretical Chemistry and Molecular Modelling (UTC2M), University of Abomey-Calavi (UAC)/Benin
gaston.kpotin@fast.uac.bj

Available online at: www.isca.in, www.isca.me
Received 24th October 2025, revised 18th January 2026, accepted 30th January 2026

Abstract

Diabetes has become a major global public health issue, with a significant rise in its prevalence, ranking among the top 10 causes of death worldwide. Various therapeutic and preventive approaches have been proposed. However, there are currently few drugs capable of counteracting the development of associated pathologies. This integrated study examines the relationship between the electronic structure and the inhibitory activity of a series of (E)-3-(2-benzylidenehydrazinyl)-5,6-diphenyl-1,2,4-triazine compounds on α-Glucosidase enzyme to propose new, more effective molecular structures. Based on the analysis of the resulting quantitative structure-activity relationship (QSAR) equation, a 2D pharmacophore was proposed. Subsequently, a new molecular structure was designed using Craig plot according to this pharmacophore. Through virtual screening of this compound, one hundred new hit molecules structures were identified and subjected to molecular docking analysis. Considering the PLP scores obtained and ADMET analysis, only six of them satisfy Lipinski's rule, among which the molecule M30 emerged as the best candidate for the treatment of type 2 diabetes.

Keywords: Diabetes, QSAR, virtual screening, molecular docking, α-Glucosidase, triazine.

Introduction

Diabetes is one of the leading causes of mortality and morbidity all over the world[1,2]. It is recognized as a life-threatening public health issue of global concern[3], due to its high prevalence, long-term complications, and the substantial cost of treatment[4]. It is a chronic metabolic disorder characterized by hyperglycemia, accompanied by a disruption in carbohydrate, lipid and protein metabolism, resulting from insufficient insulin secretion and/ or action. It is typically diagnosed when fasting blood glucose levels exceed 1.26 g/L (7 mmol/L)[5,6]. Type I and type II diabetes share similar physiopathological characteristics but differ in their underlying causes[7]. According to the International Diabetes Federation, by 2045, approximately 693 million people aged 18-99 year are projected to be living with type 2 diabetes[8]. As highlighted above, elevated blood glucose level is one of the primary indicator of diabetes. Glucose production in the body is largely driven by the enzymatic activities of glucosidase amylases, which play crucial role in breaking down starches and dietary sugars into glucose[9,10].

α-glucosidases enzymes, including maltase-glucoamylase and sucrase-isomaltase, are bound to the intestinal membrane and primarily catalyze the conversion of oligosaccharides, trisaccharides and disaccharides in glucose and other monosaccharides in the brush border of the small intestine[7,11]. Currently, several therapeutic agents are available to regulate blood glucose levels, such as metformin, thiazolidinedione and sitagliptin, which effectively improve insulin resistance. However, adverse effects, including drug resistance, acute kidney toxicity and increased heart attack risks limit widespread use of these medications, with exception of metformin, which remains the most commonly prescribed[12–14]. The search for new molecules capable of inhibiting α-glucosidases enzymes has become a major focus in the fight against type 2 diabetes, offering a promising strategy to better control blood glucose levels[15].

Significant efforts have been made by researchers to identify new bioactive molecules, either from herbal medicine sources[16–20] or through the synthesis of novel compounds[21]. Among these, (E)-3-(2-benzylidenehydrazinyl)-5,6-diphenyl-1,2,4-triazine derivatives have attracted considerable attention[22] due to their diverse biological activities, including, inhibition of maltase-glucoamylase and sucrase-isomaltase[23] and their role as α-glucosidase and α-amylase inhibitors[24]. The anti-diabetic potential of these derivatives can be further enhanced through the application of bioinformatics tools such as quantitative structure-activity relationship (QSAR) modeling, virtual screening[25], molecular docking[26] and Adsorption, Distribution, Metabolism, Excretion, and Toxicity (ADMET) analysis[27]. QSAR has become a cornerstone in modern medicinal chemistry, aiming to develop predictive statistical models that estimate the biological activity of untested compounds. Virtual

screening plays a pivotal role in drug discovery by enabling the rapid identification of promising bioactive compounds from extensive chemical libraries, thereby, streamlining the search for new therapeutic agents[28].

In this study, the QSAR study was conducted using the Klopman-Peradejordi-Gomez (KPG) approach[29], which offers the advantage of correlating biological activity with local atomic reactivity indices. This method enables the identification of specific atoms and substituents that can enhance the biological activity of the molecules. QSAR modeling, combined with virtual screening and molecular docking, was employed to propose novel pharmacophores and potential antidiabetic compounds derived from (E)-3-(2-benzylidenehydrazinyl)-5,6-diphenyl-1,2,4-triazine, targeting the α-glucosidase enzyme (PDB: 3w37).

Materials and Methods

Selection of molecules: Regarding the selection of molecules and their biological activities, the (E)-3-(2-benzylidenehydrazinyl)-5,6-diphenyl-1,2,4-triazine derivatives and their biological activities were selected from a recent study[30]. The calculated logarithmic values of their biological activities, obtained from the literature are presented in Table 1 below. The experimental data used in this part of the study correspond to the "*in vitro*" inhibitory activity on the α-Glucosidase (α-G) enzyme, characterized by IC_{50}. The common skeleton is showed in Figure-1.

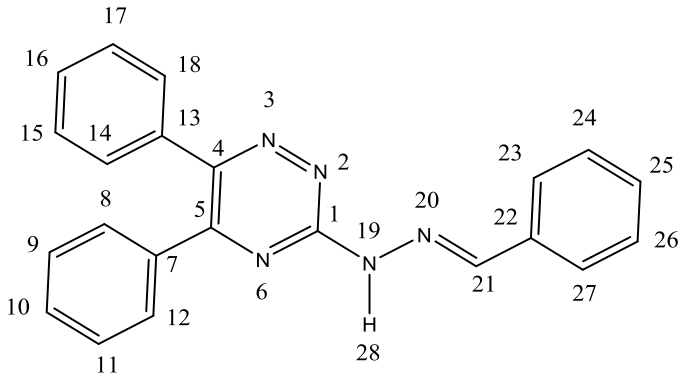

Figure-1: Numeric labelling of atoms of the core skeleton of (E)-3-(2-benzylidenehydrazinyl)-5,6-diphenyl-1,2,4-triazine derivatives.

Quantitative structures activity relationship (QSAR): For the QSAR study, the Klopman-Peradejordi-Gómez (KPG) approach has been thoroughly reviewed in several publications[29,31,32]. This method has proven to be both convincing and valuable for prediction biological activities[32–37]. The KPG approach employs a linear equation that relates the logarithm of biological activity (IC_{50}), measured either *in vivo* or *in vitro* to a set of local atomic reactivity indices (LARI) corresponding to specific atoms within the molecule.

$$\log(IC50) = a + f(LARIs) \quad (1)$$

Table-1: Derivatives of (E)-3-(2-benzylidenehydrazinyl)-5,6-diphenyl-1,2,4-triazine and their experimental inhibitory concentrations against α-Glucosidase (α-G)[30].

Mol	R_1	R_2	R_3	R_4	R_5	$\log(IC_{50})$ α-G
1	H	H	H	H	H	1.42
2	H	H	Cl	H	H	1.12
3	Cl	H	H	H	Cl	1.42
4	H	H	Cl	H	Cl	1.16
5	F	H	H	H	H	1.56
6	H	H	CF_3	H	H	1.16
7	H	H	OH	H	H	1.56
8	H	H	OH	H	OH	1.56
9	H	H	OH	OH	H	1.65
10	H	NO_2	H	H	H	1.41
11	H	OH	H	H	NO_2	1.42
12	H	NO_2	H	H	Cl	1.16
13	H	Cl	H	H	NH_2	1.56
14	H	H	OCH_3	OH	H	1.56
15	OCH_3	H	H	H	H	1.67
16	H	H	H	OCH_3	Cl	1.42
17	H	OCH_3	OCH_3	OCH_3	H	1.44
18	H	OCH_3	Br	OCH_3	H	1.42
19	OCH_3	H	Br	H	OCH_3	1.54
20	Br	H	H	OCH_3	OH	1.44
21	H	H	F	OCH3	H	1.17
22	H	H	H	H	OCH_2Ph	1.42
Standard					Acarbose	1.42

Where: a is a constant and f(LARIs) is a function of the local atomic reactivity indices (LARIs). These indices account for atom-atom electrostatic interactions, electron-donating and electron-accepting properties, the maximum charge an atom can

accommodate, and other relevant atomic characteristics. The complete expression of this equation is given as follows:

$$\log(IC50) = a + b * \log(M_D) + \sum_{o=1}^{subs} \rho_o + \sum_{i=1}^{Z}\left[e_i Q_i + f_i S_i^E + S_i S_i^N\right] + \sum_{i=1}^{Z}\sum_{m=(HOMO)^*.i}^{(HOMO-2)^*.i}\left[h_i(m)F_i(m^*) + j_i(m)S_i^E(m^*)\right] + \sum_{i=1}^{Z}\sum_{m'=(LUMO-2)^*.i}^{(LUMO+2)^*.i}\left[r_i(m')F_i(m'^*) + t_i(m')S_i^N(m'^*)\right] + \sum_{i=1}^{Z}\left[g_i\mu_i^* + k_i\eta_i^* + o_i\omega_i^* + Z_i\zeta_i^* + W_iQ_i^{*.max}\right] \quad (2)$$

Where: i. M_D: Mass of the drug. ii. ρ_o: Orientation parameter of the o-th substituent. iii. Q_i: Net charge of the atom i, iv. S_i^E, S_i^N: Electrophilic superdelocalizability and total atomic nucleophilic of atom i, respectively. v. $F_i(m^*)$: Fukui index (electron population) of atom i in an occupied molecular orbital (MO) m* or empty MO (m'*). vi. $S_i^E(m^*)$: Electrophilic superdelocalizability of occupied OM m* for atom i. vii. $S_i^N(m'^*)$: Nucleophilic superdelocalizability of empty MO m'* for atom i. viii. $\mu_i^*, \eta_i^*, \omega_i^*, \zeta_i^*, Q_i^{*.max}$ Chemical potential, local atomic hardness, local atomic electrophilicity, local atomic softness, and the maximum electronic charge atom i can accept, respectively.

Calculation: The electronic structures of the molecules were determined using Density Functional Theory (DFT) at the B3LYP/6-31G(d.p.) level, with full geometry optimization. All calculations were performed using the Gaussian 09 suite of programs.

The local atomic reactivity indices (LARIs) were computed using the custom D-CENT-QSAR program[38], which extracted the relevant numerical values from GAUSSIAN output files.

Multiple linear regression analyses (MLRA) where conducted using Statistica 10 software to establish quantitative structure-activity relationships (QSAR).

Virtual screening analysis: Virtual screening aims to computationally search the universe of potential organic molecules to identify a manageable number of virtual hits molecules[39,40]. In this study, we conducted a virtual screening to identify novel analogs based on a pharmacophore model.

The screening started from the compound depicted in Figure-4, which was proposed based on the pharmacophore structure obtained in Figure-3 and fully optimized geometrically using Gaussian software.

We utilized the InfiniSee software from BioSolveIT[41–43], to navigate vast chemical Space, including CHEMriya, eXplore, FreedomSpace, GalaXi, KnowledgeSpace and REALSpace[44].

Filtering parameters such as: target similarity (1) and minimum similarity (0.35)[45], were applied to refine the search. In InfiniSee, ECFP4 molecular fingerprint (Extended Connectivity Fingerprint with a diameter of 4) was employed to identify close analogs of the reference compound. This approach, implemented in the "Analog Hunter" mode of InfiniSee, enables the search for structurally similar molecules based on molecular fingerprint similarity, quantified using the Tanimoto similarity index[46,47].

Molecular docking: α-glucosidase (PDB ID: 3W37) enzyme complexed with acarbose was retrieved from the Protein Data Bank (PDB) for molecular docking studies[48]. Missing residues in the protein structure were added using the Genetic Optimization for Ligand Docking (GOLD) software to ensure accurate modeling of potential interactions[49,50]. The crystal-bound ligands and water molecules were removed, and hydrogen atoms were added to complete the protein structure. Both the protein and ligand structures were then converted into Mol2 format for docking. To validate the docking protocol, self-docking was performed by re-docking the native ligand into the active site. The method was considered reliable as the best-docked pose achieved a root mean square deviation (RMSD) of ≤ 2 Armstrong, indicating accurate reproduction of the experimental binding mode.

Results and Discussion

Model for predicting inhibitory activity of (E)-3-(2-benzylidenehydrazinyl)-5,6-diphenyl-1,2,4-triazine derivatives onα-Glucosidase enzyme.

The QSAR study allowed us to obtain the following regression equation:

$$\log(IC_{50}) = 2.57 - 2.34\omega_{10} + 3.09F_{19}(LUMO)^* - 1.41S_{17}^E(HOMO)^* - 0.14S_{25}^E + 0.10S_{26}^E(HOMO)^* + 1.47Q_{15}^{max} - 0.04S_{27}^N(LUMO)^* - 0.13Q_{27} - 0.61F_8(HOMO)^* - 0.21\mu_{17} - 0.15F_{24}(HOMO)^* \quad (3)$$

with n=22; R=0.99; R^2=0.99; R^2 adjusted=0.98; F (11, 10) =158.10; p <0,00000; Estimated standard error: 0.07.

Out of the 22 molecular cases studied, no outliers were detected, and no residuals were found outside the ± 2σ limit. In this equation :ω_{10} represents the propensity (electrophilicity) of atom 10 to exchange charge with an electron-accepting site, $F_{19}(LUMO)^*$ denotes the electron population (Fukui index) of the lowest unoccupied molecular orbital localized on atom 19, $S_{17}^E(HOMO)^*$ is the electrophilic superdelocalizability (electron-donating capacity) of the highest occupied orbital localized on atom 17, S_{25}^E represents the total superdelocalizability (total atomic capacity) of atom 25 to donate electrons (MO-MO interaction), $S_{26}^E(HOMO)^*$ refers to the electrophilic superdelocalizability (electron-donating capacity) of the highest occupied orbital localized on atom 26, Q_{15}^{max} indicates the maximum electronic charge that atom 15 can accept from a donor site, $S_{27}^N(LUMO)^*$ corresponds to the nucleophilic superdelocalizability (electron-accepting capacity) of the lowest unoccupied orbital localized on atom 27, Q_{27} is the net charge (electrostatic interaction) of atom 27, $F_8(HOMO)^*$ represents

the electron population (Fukui index) of the highest occupied molecular orbital localized on atom 8, μ_{17} indicates the chemical potential of atom 17, $F_{24}(HOMO)^*$ is the electron population (Fukui index) of the highest occupied molecular orbital localized on atom 24. The beta coefficients, the t-test and p-value of the eleven explanatory variables of the model are presented in Table-2.

Table-2: Beta coefficients, t-test statistics and p-value of variables in equation (3).

Variables	Beta coefficients	t(10)	p-Value
ω_{10}	-1.55	-29.33	0.000000
$F_{19}(LUMO)^*$	0.68	14.45	0.000000
$S_{17}^{E}(HOMO)^*$	-0.36	-12.04	0.000000
S_{25}^{E}	-0.48	-14.23	0.000000
$S_{26}^{E}(HOMO)^*$	0.25	8.41	0.000008
Q_{15}^{max}	0.37	8.74	0.000005
$S_{27}^{N}(LUMO)^*$	-0.19	-6.54	0.000065
Q_{27}	-0.15	-3.64	0.004554
$F_8(HOMO)^*$	-0.18	-4.71	0.000830
μ_{17}	-0.15	-4.02	0.002426
$F_{24}(HOMO)^*$	-0.11	-3.01	0.013011

Table-3 presents the correlation matrix of the eleven explanatory variables in the model. The analysis of the data in this table revealed that the strongest internal correlation is observed between variables $F_{19}(LUMO)^*$ and ω_{10}, with a correlation coefficient of 0.45.

Figure-2 represents the graph of the experimental values plotted against the calculated log(IC_{50}) values. The statistical parameters associated with equation (III) demonstrate that it is statistically significant, and the variation in the numerical values of the eleven LARIs accounts for approximately 95% confidence in the variation of the biological activity.

To suggest the type of molecular interaction implied by the presence of atoms in the equation (III), we determined the nature of their three highest occupied molecular orbitals ((HOMO-2)*, (HOMO-1)*, (HOMO)* and the three lowest unoccupied molecular orbitals (LUMO)*, (LUMO+1)*. (LUMO+2)* based on the output files of the single-point calculation.

Discussion: The values in Table-2 shows that the importance of the variables decreases in the following order : $\omega_{10}>S_{25}^{E}>S_{17}^{E}(HOMO)^*>S_{27}^{N}(LUMO)^* \approx F_8(HOMO)^*>Q_{27} \approx \mu_{17}>F_{24}(HOMO)^*>S_{26}^{E}(HOMO)^*>Q_{15}^{max}>F_{19}(LUMO)^*$.

Table-2 also indicates that the $F_{24}(Homo)^*$ index has low significance dueto its p-Value exceeding 0.005. Consequently, the statistical analysis will be based solely on the top 10 local atomic reactivity indices. In addition, given the nature of the indices involved, this process appears to be a charge-control and orbital-interaction-based analysis.

Regarding the discussion, the results indicate that the inhibitory activity of the 22 studied molecules in this series is associated with a simultaneous variation of 11 local atomic reactivity indices within the common framework. The variables-by-variable analysis (VpV) method will be employed for this study. Additionally, the Fukui indices are consistently positive ; electrophilicity, total electrophilic superdelocalizability, and partial electrophilic superdelocalizability are negative ; nucleophilic superdelocalizability is generally positive except for exceptional cases ; and the electronic chemical potential is negative. However, the VpV analysis shows that high biological activity correlates with low negative values for indices such as:

$S_{17}^{E}(HOMO)^*$,S_{25}^{E},$\mu_{17}S_{26}^{E}(HOMO)^*Q_{27}$ and high positive values for indices like : $S_{27}^{N}(LUMO)^*$, $F_8(HOMO)^*$, $F_{19}(LUMO)^*$,Q_{15}^{max}, ω_{10}.

To gain a deeper insight into the molecule under study, it is essential to conduct an analysis at the molecular level based on the results obtained from equation (III). The following section is dedicated to this aspect of the analysis. Atom 10 is a carbon atom in ring B, a high positive value of ω_{10} is achieved either by increasing the chemical potential or decreasing the hardness. This analysis suggests that atom 10 interats with an electron-rich center. Atom 17 is a carbon atom in ring A, and a low negative value of μ_{17} can be obtained by making $(HOMO)^*$ energy less negative, which makes this atom a good electron donor. Two positional cases for the $HOMO_{17}^*$ and $LUMO_{17}^*$ orbitals are observed. In both cases, these orbitals do not correspond to the $HOMO^*$ et $LUMO^*$ of the molecule, indicating that the $HOMO^*$ must be made more reactive. Consequently, atom 17 interacts with an electron-deficient center, likely, through pi-interactions, in competition with the low negative value of $S_{17}^{E}(HOMO)^*$. A low nagative value of$S_{17}^{E}(HOMO)^*$ is achieved by lowering the energy of the $(HOMO)_{17}^*$ orbital, reducing its reactivity. Therefore, atome 17 interacts with an electron-rich center. Atom 25 is a carbon atom in ring D. A low negative value of S_{25}^{E} implies interaction with an electron-rich receptor site, such as a carboxylate group. Atom 26 is a carbon atom in ring D of the common framework. Only the $(HOMO)_{26}^*$ orbital participates in the process, this orbital coincides with the molecular HOMO but the $(LUMO)_{26}$*does not mach the molecular LUMO. A large negative value of $S_{26}^{E}(HOMO)^*$ is obtained either by increasing the fukui index of $(HOMO)_{26}^*$or decreasing its energy, indicating interaction with an electron-attracting group like NO_2. Atom 27 is a carbon atom in ring D. A high positive value of $S_{27}^{N}(LUMO)^*$ is achieved either by increasing the Fukui index $LUMO_{27}^*$ or lowering its energy, making $(LUMO)_{27}^*$ more reactive.

The positive sign of the $F_8(HOMO)^*$ coefficient requires a high positive value for the index, suggesting that atom 8 is involved in an MO-MO repulsive interation with one or more orbitals of the receptor's active site, likely via pi-pi interactions. Atom 19 is a nitrogen atom in the common framework. A low positive value of $F_{19}(LUMO)^*$suggests interaction with an electron-deficient center, probably through pi-pi interactions. Atom 15 is a carbon atom in ring A. Since the energy difference between $(HOMO)_{15}^*$ and $(LUMO)_{15}^*$ is positive, obtaining a high positive value of Q_{15}^{max} requires increasing the energy of $(HOMO)_{15}^*$. This implies that atom 15 interacts with an electron-deficient center, potentially via pi-pi ou pi-σ interactions.

From all these analyses we proposed the following partial 2D pharmacophore (Figure-3).

Proposed hypothetical α-glucosidase pharmacophore-based inhibitor compound: Based on the sites indicated on this pharmacophore offigure 3, the new hypothetical antidiabetic molecule shown in figure 4was proposed using Craig plot[51]. Specifically, at sites 8, 10, 15,17,19,25, 26 and 27, different chemical substituents were positioned, exhibiting either a mesomeric electron-withdrawing effect (-M)/ an inductive electron-withdrawing effect (-I) or a mesomeric electron-donating effect (+M)/ an inductive electron-donating effect (+I), respectively.

Virtual screening analysis: As highlighted above, based on the pharmacophore-based compound, we identified one hundred (100) synthetically accessible hit molecules with similar chemical properties using InfiniSee software 6.2.0. These molecules will serve as the basis for molecular docking.

Molecular docking study: Docking protocol validation on α-Glucosidase: The root mean square deviation (RMSD) of the best pose, which has the highest affinity score of 69.0 with the site, is equal to 2 Angstrom. This RMSD confirms that our docking protocol is validated and can serve as a basis for docking the one hundred hypothetical antidiabetic compounds under study on the α-glucosidase enzyme.

Molecular docking of the one hundred hit molecules: We performed the docking process, Among the one hundred hypothetical antidiabetic molecules studied, only thirty (30) molecules exhibited affinity scores higher than the reference molecule. Therefore, these molecules are considered to have a stronger affinity for the 3W37 receptor site compared to the reference. These thirty compounds will be subjected to ADMET analysis (Sup data).

Table-3: Correlation coefficients for variables appearing in equation (3)

Variables	$\mathbf{F_8}$ $\mathbf{(HOMO)^*}$	$\boldsymbol{\omega_{10}}$	$\mathbf{Q_{15}^{max}}$	$\mathbf{S_{17}^E}$ $\mathbf{(HOMO)^*}$	$\boldsymbol{\mu_{17}}$	$\mathbf{F_{19}}$ $\mathbf{(LUMO)^*}$	$\mathbf{F_{24}}$ $\mathbf{(HOMO)^*}$	$\mathbf{S_{25}^E}$	$\mathbf{S_{26}^E}$ $\mathbf{(HOMO)^*}$	$\mathbf{Q_{27}}$
ω_{10}	0.10	1.00								
Q_{15}^{max}	0.12	0.42	1.00							
$S_{17}^{E}(HOMO)^*$	0.00	0.00	0.08	1.00						
μ_{17}	0.00	0.00	0.00	0.06	1.00					
$F_{19}(LUMO)^*$	0.26	0.45	0.21	0.01	0.00	1.00				
$F_{24}(HOMO)^*$	0.04	0.02	0.01	0.03	0.12	0.07	1.00			
S_{25}^{E}	0.12	0.00	0.03	0.07	0.18	0.00	0.05	1.00		
$S_{26}^{E}(HOMO)^*$	0.00	0.00	0.03	0.03	0.00	0.01	0.05	0.00	1.00	
Q_{27}	0.01	0.17	0.00	0.11	0.22	0.03	0.00	0.01	0.02	1.00
$S_{27}^{N}(LUMO)^*$	0.00	0.00	0.02	0.00	0.01	0.03	0.00	0.01	0.20	0.00

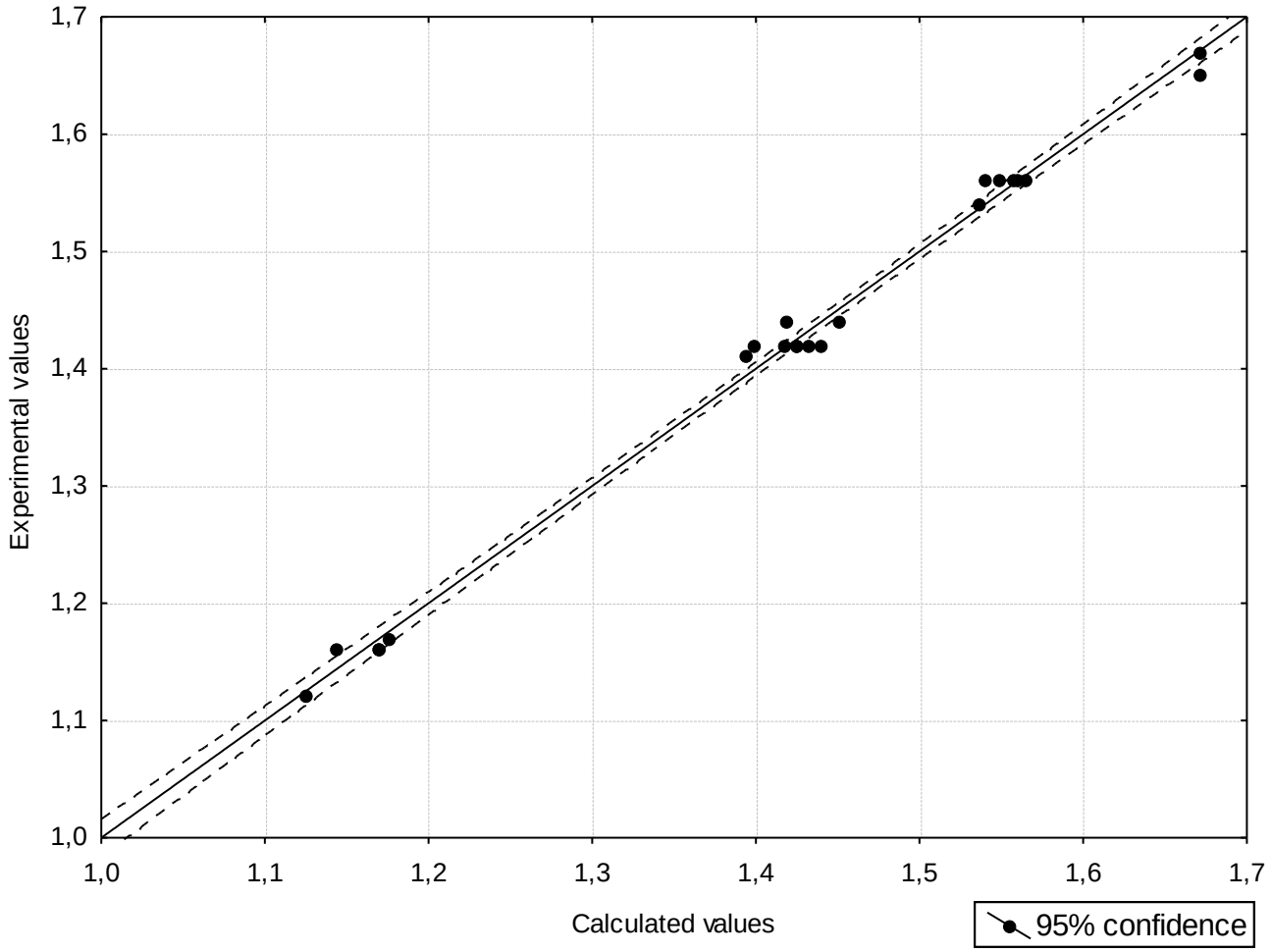

Figure-2: Graph of the experimental values plotted against the calculated log (IC50) values. Dotted lines indicate the 95% confidence interval in the correlation.

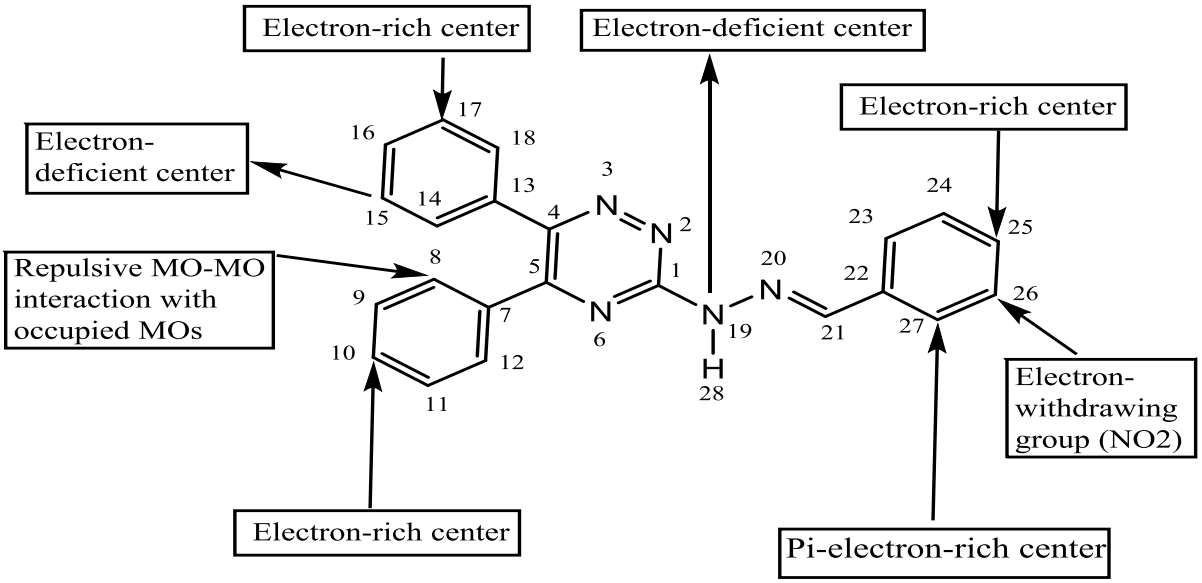

Figure-3: 2D partial pharmacophore of (E)-3-(2-benzylidenehydrazinyl)-5,6-diphenyl-1,2,4-triazine derivatives with the α-Glucosidase enzyme.

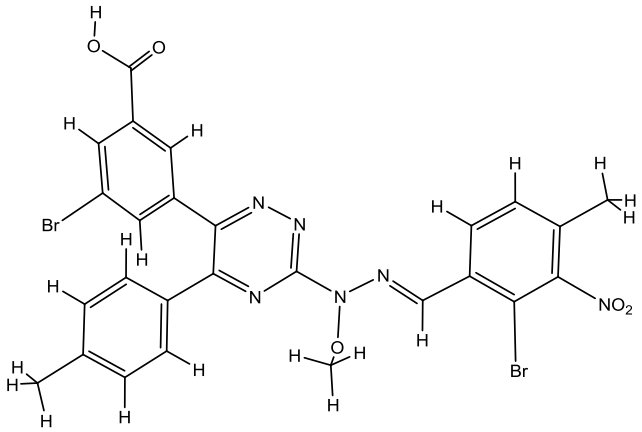

Figure-4: Molecule structure of the pharmacophore-based compound.

Molecular docking analysis

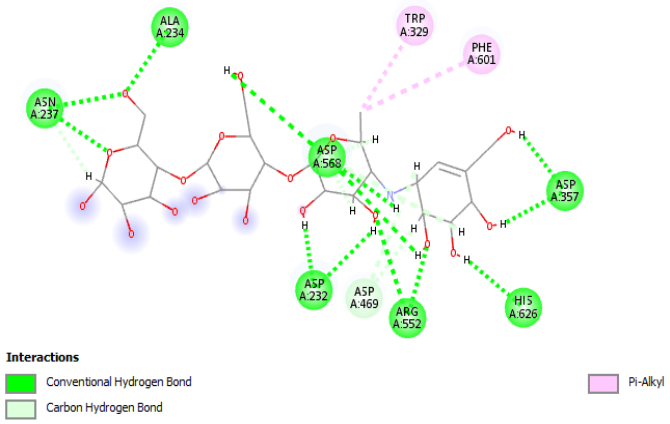

Figure-5: The crystal ligand in the active site of the enzyme 3W37.

Figure-5 illustrates the docking configuration of the crystal ligand within the active site of the 3W37 enzyme. The ligand is stabilized through multiple interactions, including Van der Waals forces and conventional hydrogen bonds with residues such as ASN 237, ASP 232, ASP 357, HIS 626, ARG 552, ASP 568 and ALA 234. Pi-alkyl interactions are also evident, particularly involving residues like TRP 329 and PHE 601. The crystal ligand's optimal alignment within the binding pocket underscores the structural complementarity of the enzyme's active site and will be useful for evaluating the bending efficacy of hypothetical compounds.

Figure-6 highlighted the interaction of the pharmacophore-based compound within the active site of the 3W37 enzyme. Key interactions include pi-cation and hydrogen bond with residue LYS 506. These interactions stabilize the ligand within the bending site, indicating a favorable orientation for inhibitory activity. In addition, pi-pi stacking interactions with TRP 432 and PHE 476 suggest strong hydrophobic contribution to binding affinity. The structural alignment of the pharmacophore validates its design based on QSAR analyses.

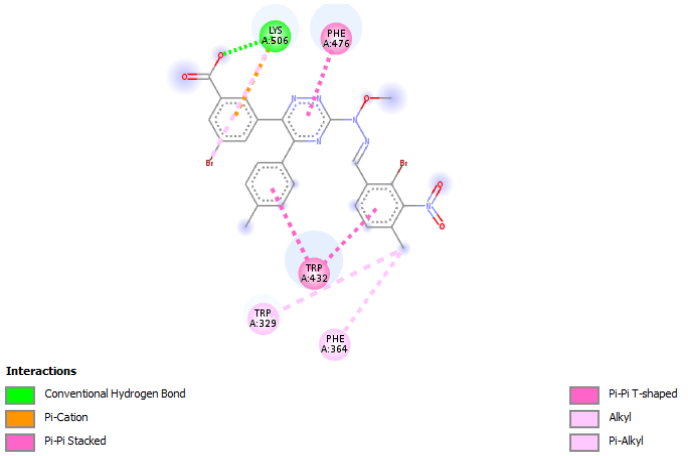

Figure-6: Docking of the pharmacophore-based compound.

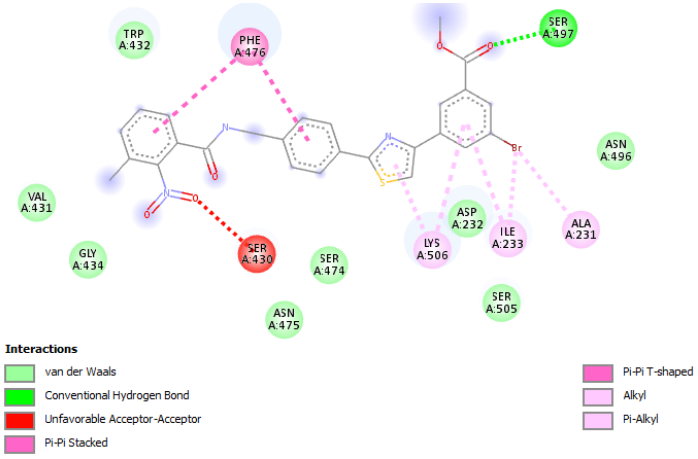

Figure-7: Molecular docking of hypothetical compound M9.

Figure-7 demonstrates how M9 fits into the active site, forming several key interactions such as Van der Waals interactions with VAL 431, GLY 434, ASN 475, SER 474, ASN 475, TRP 432, SER 505, ASN 496, ASP 232 and conventional hydrogen bonding with SER 497, which enhance its binding. Favorable pi-stacking interactions. Strengthen binding, while unfavorable interactions may affect binding efficiency.

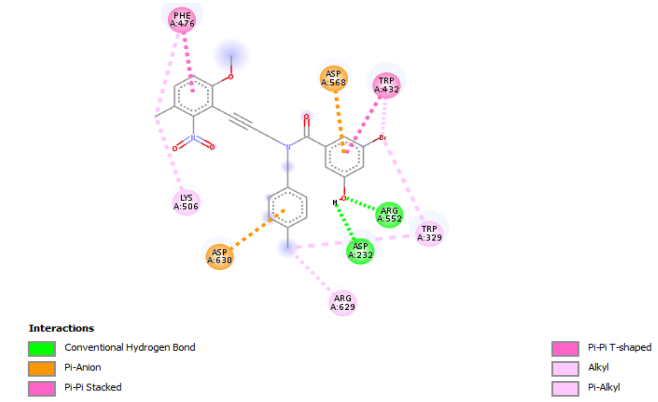

Figure-8: Molecular docking of hypothetical compound M15.

Figure-8 shows how M15 fits into the active site.M15 exhibits a strong docking profile, with critical interactions including hydrogen bonds with ASP 232, ARG 552 and pi-alkyl interactions with TRP 329, LYS 506. Notably, PHE 476 forms pi-pi stacking contacts contributing to the overall stability of the compound in the active site. The compound's configuration suggests enhanced binding through its electron-rich aromatic rings, polar interaction which interact with residues such as ASP 630 and ASP 568.

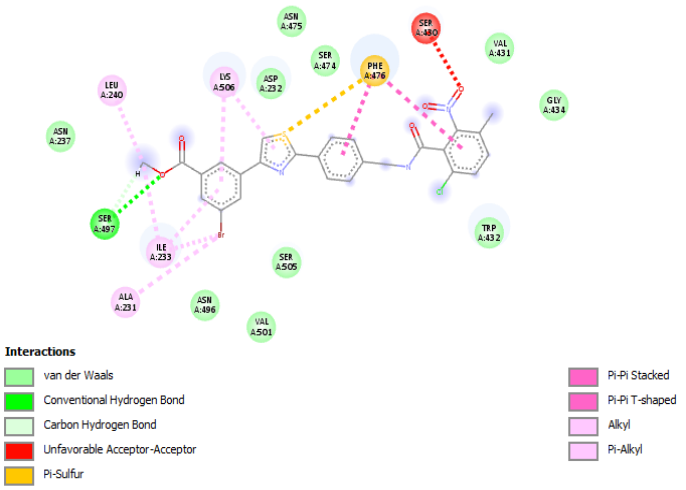

Figure-9: Molecular docking of hypothetical compound M18.

Figure-9 demonstrates how M18 fits into the active site.The molecule M18 forms robust interactions within the active site, including conventional hydrogen bonds with ASP 232 and ASN 475. Hydrophobic contacts, particularly pi-alkyl interactions with ILE 233, enhance its binding. Additionally, the orientation of its substituents suggests potential for strong receptor affinity. TRP 432 and PHE 476 participate in pi-pi shaped interactions, enhancing the binding through aromatic stacking. The molecule's binding conformation reflects its ability to maintain a stable ligand-receptor complex.

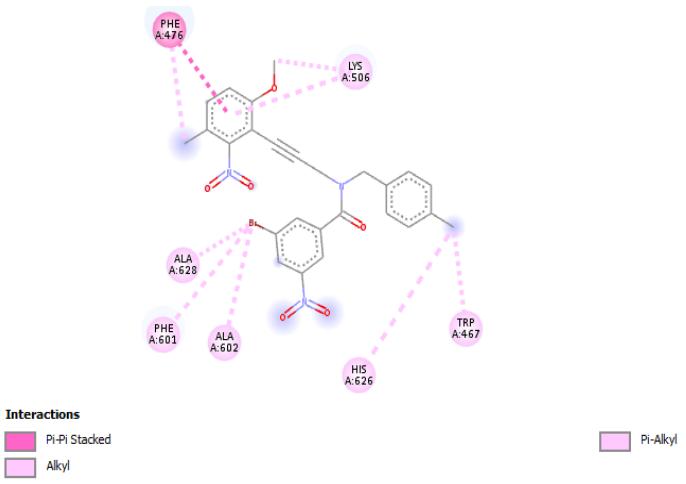

Figure-10: Molecular docking of hypothetical compound M19.

Figure-10 shows M19 designed to exploit aromatic stacking and hydrophobic interactions. PHE 476 engages in multiple pi-pi stacking interactions with the ligand's aromatic groups, providing strong aromatic stabilization. TRP 467 forms pi-alkyl interactions, adding to the hydrophobic character of the binding pocket which reinforces its binding affinity. While the interactions are strong, the absence of hydrogen bonds might limit its binding strength.

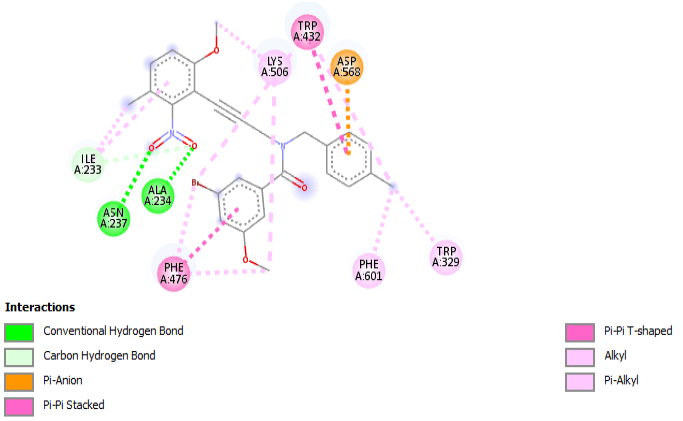

Figure-11: Molecular docking of hypothetical compound M29.

Figure-11 demonstrates how M29 fits into the active site. The Molecule M29 interacts effectively within the enzyme's active site, forming Van der Waals interactions with residues such as ILE 233, LYS 506 and pi-pi stacking contacts with PHE 476 and PHE 601.these interactions provide an aromatic stabilization of the compound. A notable interaction includes hydrogen bonding with ASN 237, which positions the molecule optimally for inhibition. The arrangement of functional groups suggests M29 may be an effective competitive inhibitor.

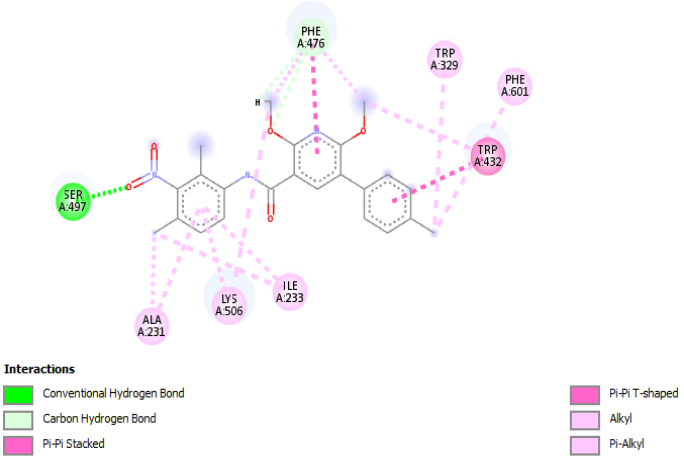

Figure-12: Molecular docking of hypothetical compound M30.

Figure-12 shows how M30 fits into the active site.M30 identified as the best candidate, forms extensive polar and nonpolar interactions such as: strong aromatic interactions through pi-pi stacking and T-shaped interactions, and effective hydrogen bonding with SER 497. This later interaction provides

specificity to the binding. The molecule's docking conformation maximizes interactions with hydrophobic residues such as LYS 506 and ILE 233, critical for stability and high PLP scores. The precise orientation of this molecule's substituents reflects its high binding efficiency and supports its selection as the most active compound.

In conclusion, the molecular docking analyses of the proposed pharmacophore-based compound and its derivates demonstrated their strong potential as α-Glucosidase inhibitors. Key interactions with the active site residues, including hydrogen bonds, Van der Waals forces, and pi-pi stacking, highlight the compound's capacity to establish stable ligand-receptor complexes. The consistency of these findings with QSAR predictions and ADME analyses further validates the proposed compounds as viable candidates for type 2 diabetes treatment. M30, in particular, holds significant promise for addressing hyperglycemia-related dysfunction.

Hypothetical molecules obtained based on ADMET analysis: For the final selection of more active compounds targeting the 3W37 receptor, the Lipinski's rule was applied. This rule involves selecting only molecules that meet the following criteria: molecular weight (MW) ≤500, a (log(P), MLOGP) ≤5, no more than 10 hydrogen bond acceptors acceptor (N or O atoms), and no more than 5 hydrogen bond donor (NH or OH groups). Based on the results obtained (Table-4) for the proposed hypothetical molecules, the Lipinski's rule confirms that all of the six (06) molecules retained after ADMET analysis exhibits favorable solubility and permeability, making them potential candidate molecules for type 2 diabetes treatment. To evaluate the physicochemical properties of the proposed hypothetical compounds, Swiss ADME was utilized. Figure-13 represents the six molecules that satisfied to the Lipinski's rule.

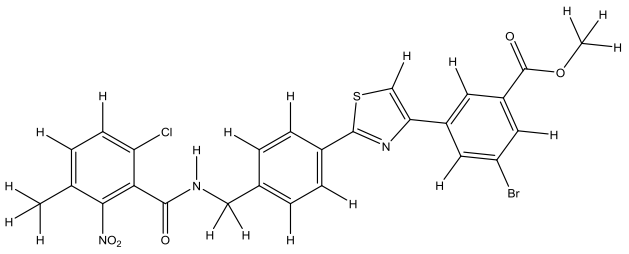

M9

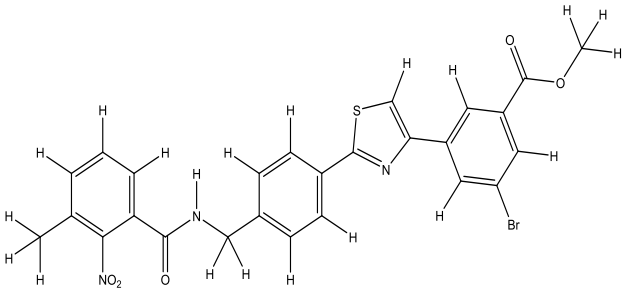

M18

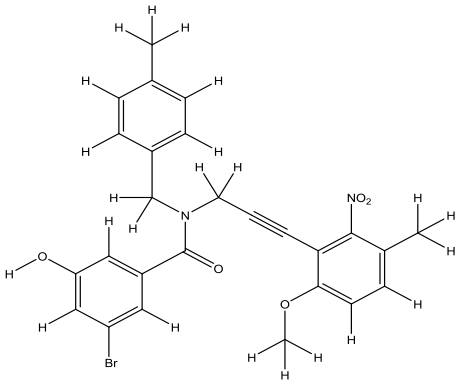

M15

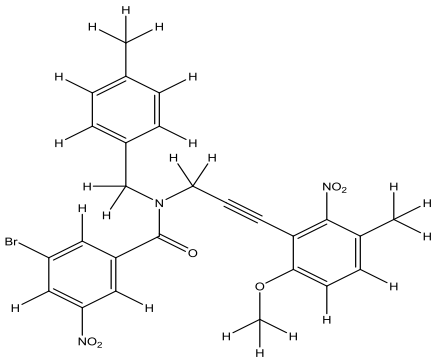

M19

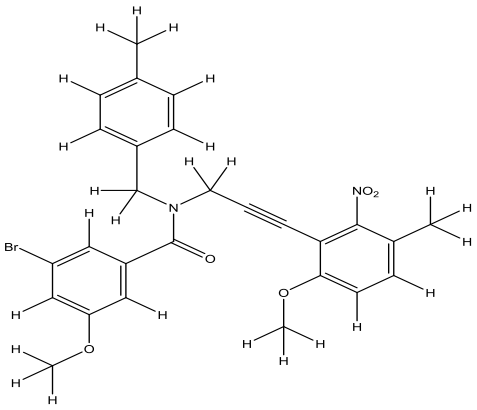

M29

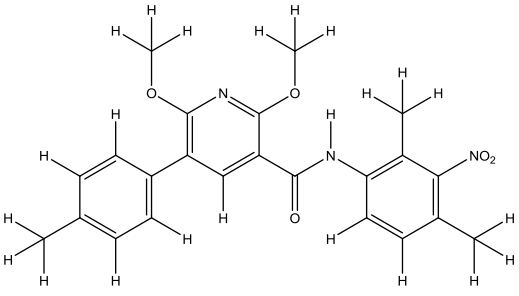

M30

Figure-13: 2D representation of hypothetical compounds obtained based on ADMET analysis.

Table-4: Physicochemical propriety, lipophilicity and druglikeness.

Molecules	Partition coefficient log(P) Or Log $P_{o/w}$ (MLOGP)	Molecular weight (Dalton)	Hydrogen bond donor	Hydrogen bond acceptors	Number of rotable bonds	Rule-of-five of Lipinski
M9	3.31	567.43	2	6	9	Yes; 1 violation: MW>500
M15	3.85	524.38	2	5	7	Yes; 1 violation: MW>500
M18	3.50	601.88	2	6	9	Yes; 1 violation: MW>500
M19	3.50	554.39	2	6	8	Yes; 1 violation: MW>500
M29	4.04	538.41	1	5	8	Yes; 1 violation: MW>500
M30	2.63	422.45	2	6	7	Yes; 0 violation

Conclusion

The QSAR study conducted in this work enable us to establish statistically significant relationships between the variation of biological activities of a series of triazines molecules and the variation of numerical values of a set of local atomic reactivity indices. Analysis derived from this mathematical relationship allowed us to propose a 2D pharmacophore. Since the analyses were performed at the molecular level, the resulting model demonstrated that the process is governed by orbital and charge control.

A hypothetical molecule was designed based on this pharmacophore using Craig plot, which served as the foundation for virtual screening analysis. From this, one hundred hit compounds were identified and subsequently docked with the active site of the 3W37 enzyme using GOLD software. After filtering the molecules based on PLP scores obtained and ADMET analysis, only six of them satisfy Lipinski's rule. Among these, the molecule named M30 emerged as the best candidate for the treatment of type 2 diabetes. Thus, the challenge of managing high blood glucose levels and associated dysfunctions linked to hyperglycemia could potentially be addressed following the synthesis and application of these novel drug compounds.

References

1. Ismail, S.; Chandel, T. I.; Ramakrishnan, J.; Khan, R. H.; Poomani, K.; Devarajan, N. (2023). Phytochemical Profiling, Human Insulin Stability and Alpha Glucosidase Inhibition of Gymnema Latifolium Leaves Aqueous Extract: Exploring through Experimental and in Silico Approach. *Comput. Biol. Chem.*, 107, 107964. https://doi.org/10.1016/j.compbiolchem.2023.107964.

2. Thabet, H. K.; Abusaif, M. S.; Imran, M.; Helal, M. H.; Alaqel, S. I.; Alshehri, A.; Mohd, A. A.; Ammar, Y. A.; Ragab, A. (2024). Discovery of Novel 6-(Piperidin-1-Ylsulfonyl)-2H-Chromenes Targeting α-Glucosidase, α-Amylase, and PPAR-γ: Design, Synthesis, Virtual Screening, and Anti-Diabetic Activity for Type 2 Diabetes Mellitus. *Comput. Biol. Chem.*, 111, 108097. https://doi.org/10.1016/j.compbiolchem.2024.108097.

3. Abbasi, I.; Nadeem, H.; Saeed, A.; Kharl, H. A. A.; Tahir, M. N.; Naseer, M. M. (2021). Isatin-Hydrazide Conjugates as Potent α-Amylase and α-Glucosidase Inhibitors: Synthesis, Structure and in Vitro Evaluations. *Bioorganic Chem.*, *116*, 105385. https://doi.org/10.1016/j.bioorg.2021.105385.

4. Ganwir, P.; Bhadane, R.; Chaturbhuj, G. U. (2024). In-Silico Screening and Identification of Glycomimetic as Potential Human Sodium-Glucose Co-Transporter 2 Inhibitor. *Comput. Biol. Chem.*, 110, 108074. https://doi.org/10.1016/j.compbiolchem.2024.108074.

5. Rigalleau, V.; Monlun, M.; Foussard, N.; Blanco, L. and Mohammedi, K. (2020). Diagnostic Du Diabète. *EMC - AKOS Traité Médecine*, 24(1), 1–7.

6. Gupta, M. K. and Vadde, R. (2019). Identification and Characterization of Differentially Expressed Genes in Type 2 Diabetes Using in Silico Approach. *Comput. Biol. Chem.*, 79, 24–35. https://doi.org/10.1016/j.compbiolchem.2019.01.010.

7. Shamim, S.; Khan, K. M.; Ullah, N.; Chigurupati, S.; Wadood, A.; Ur Rehman, A.; Ali, M.; Salar, U.; Alhowail, A.; Taha, M. and Perveen, S. (2020). Synthesis and Screening of (E)-3-(2-Benzylidenehydrazinyl)-5,6-Diphenyl-1,2,4-Triazine Analogs as Novel Dual Inhibitors of α-Amylase and α-Glucosidase. *Bioorganic Chem.*, 101, 103979. https://doi.org/10.1016/j.bioorg.2020.103979.

8. Cho, N. H.; Karuranga, S.; Huang, Y.; Da Rocha Fernandes, J. D.; Ohlrogge, A. W. and Malanda, B. (2018). IDF Diabetes Atlas: Global Estimates of Diabetes Prevalence for 2017 and Projections for 2045. *Diabetes Res. Clin. Pract.*, 138, 271–281. https://doi.org/10.1016/j.diabres.2018.02.023.

9. He, Q.; Han, C.; Li, G.; Guo, H.; Wang, Y.; Hu, Y.; Lin, Z. and Wang, Y. (2020). In Silico Design Novel (5-Imidazol-2-Yl-4-Phenylpyrimidin-2-Yl)[2-(2-Pyridylamino)Ethyl] Amine Derivatives as Inhibitors for Glycogen Synthase Kinase 3 Based on 3D-QSAR, Molecular Docking and Molecular Dynamics Simulation. *Comput. Biol. Chem.*, *88*, 107328. https://doi.org/10.1016/j.compbiolchem.2020.107328.

10. Menteşe, E.; Baltaş, N. and Emirik, M. (2020). Synthesis, α-Glucosidase Inhibition and in Silico Studies of Some 4-(5-Fluoro-2-Substituted-1H-Benzimidazol-6-Yl) Morpholine Derivatives. *Bioorganic Chem.*, 101, 104002. https://doi.org/10.1016/j.bioorg.2020.104002.

11. Kan, L.; Capuano, E.; Fogliano, V.; Verkerk, R.; Mes, J. J.; Tomassen, M. M. M. and Oliviero, T. (2021). Inhibition of α-Glucosidases by Tea Polyphenols in Rat Intestinal Extract and Caco-2 Cells Grown on Transwell. *Food Chem.*, 361, 130047. https://doi.org/10.1016/j.foodchem.2021.130047.

12. Prince Makarios Paul, S.; Parimala Devi, D.; Nancy Sukumar, A.; Praveena, G.; Jeba Beula, R. and Abiram, A. (2024). Theoretical Insights on the Interaction between P-Synephrine and Metformin: A DFT, QTAIM and Drug-Likeness Investigation. *Comput. Theor. Chem.*, 1233, 114473. https://doi.org/10.1016/j.comptc.2024.114473.

13. Hu, C. and Jia, W. (2019). Therapeutic Medications against Diabetes: What We Have and What We Expect. *Adv. Drug Deliv. Rev.*, 139, 3–15. https://doi.org/10.1016/j.addr.2018.11.008.

14. Salehi; Ata; V. Anil Kumar; Sharopov; Ramírez-Alarcón; Ruiz-Ortega; Abdulmajid Ayatollahi; Tsouh Fokou; Kobarfard; Amiruddin Zakaria; Iriti; Taheri; Martorell; Sureda; Setzer; Durazzo; Lucarini; Santini; Capasso; Ostrander; Atta-ur-Rahman; Choudhary; Cho; Sharifi-Rad. (2019). Antidiabetic Potential of Medicinal Plants and Their Active Components. *Biomolecules*, 9(10), 551. https://doi.org/10.3390/biom9100551.

15. Katsila, T.; Spyroulias, G. A.; Patrinos, G. P. and Matsoukas, M. T. (2016). Computational Approaches in Target Identification and Drug Discovery. *Comput. Struct. Biotechnol. J.*, 14, 177–184. https://doi.org/10.1016/j.csbj.2016.04.004.

16. Nguyen Vo, T. H.; Tran, N.; Nguyen, D. and Le, L. (2016). An in Silico Study on Antidiabetic Activity of Bioactive Compounds in Euphorbia Thymifolia Linn. *SpringerPlus*, 5(1), 1359. https://doi.org/10.1186/s40064-016-2631-5.

17. Rao, M. M. V. and Hariprasad, T. P. N. (2021). In Silico Analysis of a Potential Antidiabetic Phytochemical Erythrin against Therapeutic Targets of Diabetes. *Silico Pharmacol.*, 9(1), 5. https://doi.org/10.1007/s40203-020-00065-8.

18. Das, K.; Iyer, K. R.; Orfali, R.; Asdaq, S. M. B.; Alotaibi, N. S.; Alotaibi, F. S.; Alshehri, S.; Quadri, M. S. A.; Almarek, A.; Makhashin, N. B.; Alrashed, A. A.; Mohzari, Y. A.; Ghoneim, M. (2023). In Silico Studies and Evaluation of in Vitro Antidiabetic Activity of Berberine from Ethanol Seed Extract of Coscinium Fenestratum (Gaertn.) Colebr. *J. King Saud Univ. Sci.*, 35(5), 102666. https://doi.org/10.1016/j.jksus.2023.102666.

19. Gomes, A. F. T.; De Medeiros, W. F.; De Oliveira, G. S.; Medeiros, I.; Maia, J. K. D. S.; Bezerra, I. W. L.; Piuvezam, G.; Morais, A. H. D. A. (2022). In Silico Structure-Based Designers of Therapeutic Targets for Diabetes Mellitus or Obesity: A Protocol for Systematic Review. *PLOS ONE*, 17(12), e0279039. https://doi.org/10.1371/journal.pone.0279039.

20. Reetu, R.; Garg, A.; Roy, K. K.; Roy, A.; Gupta, S. and Malakar, C. C. (2022). In-Silico Studies for Targeting PPARγ for the Type II Diabetes Mellitus. *Mater. Today Proc.*, 57, 44–48. https://doi.org/10.1016/j.matpr.2022.01.299.

21. Bharathi, A.; Roopan, S. M.; Vasavi, C. S.; Munusami, P.; Gayathri, G. A.; Gayathri, M. (2014). *In Silico* Molecular Docking and *In Vitro* Antidiabetic Studies of Dihydropyrimido[4,5-*a*]Acridin-2-Amines. *BioMed Res. Int.*, 1–10. https://doi.org/10.1155/2014/971569.

22. Aggarwal, R. and Sumran, G. (2020). An Insight on Medicinal Attributes of 1,2,4-Triazoles. *Eur. J. Med. Chem.*, 205, 112652. https://doi.org/10.1016/j.ejmech.2020.112652.

23. Tannous, S.; Stellbrinck, T.; Hoter, A. and Naim, H. Y. (2023). Interaction between the α-Glucosidases, Sucrase-Isomaltase and Maltase-Glucoamylase, in Human Intestinal Brush Border Membranes and Its Potential Impact on Disaccharide Digestion. *Front. Mol. Biosci.*, 10, 1160860. https://doi.org/10.3389/fmolb.2023.1160860.

24. Yeye, E. O.; Kanwal; Mohammed Khan, Khalid.; Chigurupati, S.; Wadood, A.; Ur Rehman, A.; Perveen, S.; Kannan Maharajan, M.; Shamim, S.; Hameed, S.; Aboaba, S. A.; Taha, M. (2020). Syntheses, in Vitro α-Amylase and α-Glucosidase Dual Inhibitory Activities of 4-Amino-1,2,4-Triazole Derivatives Their Molecular Docking and Kinetic Studies. *Bioorg. Med. Chem.*, 28(11), 115467. https://doi.org/10.1016/j.bmc.2020.115467.

25. Gupta, S.; Baweja, G. S.; Singh, S.; Irani, M.; Singh, R.; Asati, V. (2023). Integrated Fragment-Based Drug Design and Virtual Screening Techniques for Exploring the Antidiabetic Potential of Thiazolidine-2,4-Diones: Design, Synthesis and in Vivo Studies. *Eur. J. Med. Chem.*, 261, 115826. https://doi.org/10.1016/j.ejmech.2023.115826.

26. Mrabti, N. N.; Mrabti, H. N.; Mohammed, E.R.; Dguigui, K.; Doudach, L.; Khalil, Z.; Bouyahya, A.; Zengin, G.; Elhallaoui, M. (2022). Molecular Docking and QSAR Studies for Modeling the Inhibitory Activity of Pyrazole-Benzimidazolone Hybrids as Novel Inhibitors of Human 4-

Hydroxyphenylpyruvate Dioxygenase Against Type I Tyrosinemia Disease. *Biointerface Res. Appl. Chem.*, 13 (1), 38. https://doi.org/10.33263/BRIAC131.038.

27. Verma, J.; Khedkar, V. and Coutinho, E. (2010). 3D-QSAR in Drug Design - A Review. *Curr. Top. Med. Chem.*, 10 (1), 95–115. https://doi.org/10.2174/15680 2610790232260.

28. Moshawih, S.; Bu, Z. H.; Goh, H. P.; Kifli, N.; Lee, L. H.; Goh, K. W. and Ming, L. C. (2024). Consensus Holistic Virtual Screening for Drug Discovery: A Novel Machine Learning Model Approach. *J. Cheminformatics*, 16(1), 62. https://doi.org/10.1186/s13321-024-00855-8.

29. Gómez-Jeria, J. S. (2017). 45 Years of the KPG Method: A Tribute to Federico Peradejordi. *J. Comput. Methods Mol. Des.*, 7(1), 17–37.

30. Shamim, S.; Khan, K. M.; Ullah, N.; Chigurupati, S.; Wadood, A.; Ur Rehman, A.; Ali, M.; Salar, U.; Alhowail, A.; Taha, M. and Perveen, S. (2020). Synthesis and Screening of (E)-3-(2-Benzylidenehydrazinyl)-5,6-Diphenyl-1,2,4-Triazine Analogs as Novel Dual Inhibitors of α-Amylase and α-Glucosidase. *Bioorganic Chem.*, 101, 103979. https://doi.org/10.1016/j.bioorg.2020.103979.

31. Gómez Jeria, J. S. (2013). A New Set of Local Reactivity Indices within the Hartree-Fock-Roothaan and Density Functional Theory Frameworks. *Can. Chem. Trans.*, 1(1), 25–55.

32. Gómez Jeria, J. S. and Flores-Catalán, M. (2013). Quantum-Chemical Modeling of the Relationships between Molecular Structure and In Vitro Multi-Step, Multimechanistic Drug Effects. HIV-1 Replication Inhibition and Inhibition of Cell Proliferation as Examples. *Can. Chem. Trans.*, 1(3), 215–237. https://doi.org/DOI: 10.13179/canchemtrans.2013.01.03.0040.

33. Gómez-Jeria, J. S.; Kpotin, G.; Kuevi, U.; Mensah, J.-B.; De Gautier, K. (2017). A Theoretical Study of the Relationships between Electronic Structure and Inhibitory Effects of Caffeine Derivatives on Neoplastic Transformation. *Int. Res. J. Pure Appl. Chem.*, 14, 1–10. https://doi.org/10.9734/IRJPAC/2017/32694.

34. Kpotin, G. A.; Bédé, A. L.; Houngue-Kpota, A.; Anatovi, W.; Kuevi, U. A.; Atohoun, G. S.; Mensah, J.-B.; Gómez-Jeria, J. S. and Badawi, M. (2019). Relationship between Electronic Structures and Antiplasmodial Activities of Xanthone Derivatives: A 2D-QSAR Approach. *Struct. Chem.*, 30(6), 2301–2310. https://doi.org/10.1007/s11224-019-01333-w.

35. Kpotin, G.; Atohoun, S. Y. G.; Kuevi, A. U.; Kpota-Hounguè, A.; Mensah, J.-B.; Gómez Jeria, J. S. (2016). A Quantum-Chemical Study of the Relationships between Electronic Structure and Trypanocidal Activity against Trypanosoma Brucei Brucei of a Series of Thiosemicarbazone Derivatives. *Pharm. Lett.*, 8(17), 215–222.

36. Kpotin, A. G.; Kankinou, G.; Kuevi, U.; Gómez Jeria, J. S.; Mensah, J.B. (2017). A Theoretical Study of the Relationships between Electronic Structure and Inhibitory Effects of Caffeine Derivatives on Neoplastic Transformation. *Int. Res. J. Pure Appl. Chem.*, 14(1), 1–10. https://doi.org/10.9734/IRJPAC/2017/32694.

37. Kankinou, S. G.; Yildiz, M.; Kocak, A. (2023). Exploring Potential *Plasmodium* Kinase Inhibitors: A Combined Docking, MD and QSAR Studies. *J. Biomol. Struct. Dyn.*, 1–11. https://doi.org/10.1080/07391102.2023.2249111.

38. D-Cent-QSAR: (2014). A Program to Generate Local Atomic Reactivity Indices from Gaussian 03 Log Files. 1.0,2014.

39. Müller, J.; Klein, R.; Tarkhanova, O.; Gryniukova, A.; Borysko, P.; Merkl, S.; Ruf, M.; Neumann, A.; Gastreich, M.; Moroz, Y. S.; Klebe, G. and Glinca, S. (2022). Magnet for the Needle in Haystack: "Crystal Structure First" Fragment Hits Unlock Active Chemical Matter Using Targeted Exploration of Vast Chemical Spaces. *J. Med. Chem.*, *65* (23), 15663–15678. https://doi.org/10.1021/acs.jmedchem.2c00813.

40. Beroza, P.; Crawford, J. J.; Ganichkin, O.; Gendelev, L.; Harris, S. F.; Klein, R.; Miu, A.; Steinbacher, S.; Klingler, F.-M.; Lemmen, C. (2022). Chemical Space Docking Enables Large-Scale Structure-Based Virtual Screening to Discover ROCK1 Kinase Inhibitors. *Nat. Commun.*, 13 (1), 6447. https://doi.org/10.1038/s41467-022-33981-8.

41. Tan, L.; Wu, C.; Zhang, J.; Yu, Q.; Wang, X.; Zhang, L.; Ge, M.; Wang, Z.; Ouyang, L.; Wang, Y. (2023). Design, Synthesis, and Biological Evaluation of Heterocyclic-Fused Pyrimidine Chemotypes Guided by X-Ray Crystal Structure with Potential Antitumor and Anti-Multidrug Resistance Efficacy Targeting the Colchicine Binding Site. *J. Med. Chem.*, 66(5), 3588–3620. https://doi.org/10.1021/acs.jmedchem.2c02115.

42. Salari-jazi, A.; Mahnam, K.; Sadeghi, P.; Damavandi, M. S. and Faghri, J. (2021). Discovery of Potential Inhibitors against New Delhi Metallo-β-Lactamase-1 from Natural Compounds: In Silico-Based Methods. *Sci. Rep.*, 11(1), 2390. https://doi.org/10.1038/s41598-021-82009-6.

43. infiniSee Version (2024). Biosolveit. www.biosolveit.de/infiniSee (accessed 2025-02-23).

44. Schmidt, R.; Klein, R.; Rarey, M. (2022). Maximum Common Substructure Searching in Combinatorial Make-on-Demand Compound Spaces. *J. Chem. Inf. Model.*, 62 (9), 2133–2150. https://doi.org/10.1021/acs.jcim.1c00640.

45. Namasivayam, V.; Silbermann, K.; Pahnke, J.; Wiese, M. and Stefan, S. M. (2021). Scaffold Fragmentation and Substructure Hopping Reveal Potential, Robustness, and Limits of Computer-Aided Pattern Analysis (C@PA). *Comput. Struct. Biotechnol. J.*, 19, 3269–3283. https://doi.org/10.1016/j.csbj.2021.05.018.

46. Fligner, M. A.; Verducci, J. S. and Blower, P. E. (2002). A Modification of the Jaccard–Tanimoto Similarity Index for Diverse Selection of Chemical Compounds Using Binary Strings. *Technometrics*, 44(2), 110–119. https://doi.org/10.1198/004017002317375064.

47. Bajusz, D.; Rácz, A.; Héberger, K. (2015). Why Is Tanimoto Index an Appropriate Choice for Fingerprint-Based Similarity Calculations?. *J. Cheminformatics*, 7(1), 20. https://doi.org/10.1186/s13321-015-0069-3.

48. Tagami, T.; Yamashita, K.; Okuyama, M.; Mori, H.; Yao, M. and Kimura, A. (2013). Molecular Basis for the Recognition of Long-Chain Substrates by Plant α-Glucosidases. *J. Biol. Chem.*, 288(26), 19296–19303. https://doi.org/10.1074/jbc.M113.465211.

49. Genetic Optimization for Ligand Docking (GOLD) (2022). Solutions Software Gold. https://www.ccdc.cam.ac.uk/Solutionssoftware/gold/?utm_source=chatgpt.com (accessed 2022-09-09).

50. Verdonk, M. L.; Cole, J. C.; Hartshorn, M. J.; Murray, C. W.; Taylor, R. D. (2003). Improved Protein–Ligand Docking Using GOLD. *Proteins Struct. Funct. Bioinforma.*, *52* (4), 609–623. https://doi.org/10.1002/ prot.10465.

51. Graham, L. P. (2013). *AN Introduction to Medicinal Chemistry*. 5th ed.; Oxford, University Press: Great Clarendon Street, Oxford, OX2 6DP, United Kingdom.